Chapter 3

NNLO Analysis of Singlet and Non-singlet Structure Functions in the DGLAP Approach

3.1 Introduction

Structure functions in lepton-nucleon DIS are the entrenched observables exploring QCD. They are defined as convolution of the universal parton momentum distributions and coefficient functions, which contain information about the boson-parton interaction. Therefore the structure functions provide exclusive information about the deep structure of hadrons and most importantly, they form the backbone of our knowledge of the parton densities, which are indispensable for analyses of hard scattering processes. Thus the measurements of the structure functions allow perturbative QCD to be precisely tested. The standard and the basic tool for theoretical investigation of DIS structure functions are the DGLAP evolution equations [1-4]. Therefore the solutions of DGLAP evolution equations give quark and gluon distribution functions which ultimately produce proton, neutron and deuteron structure functions.

The solutions of the unpolarized DGLAP equation for the QCD evolution of structure functions have been discussed considerably over the past years. The standard and the most extensively used procedure of studying the hadron structure functions is via the numerical solution of these equations [5-10], with excellent agreement with the DIS data over a wide kinematic region in x and Q^2. However, apart from the

numerical solution, there is the alternative approach of studying analytically these equations at small-x. Although exact analytic solutions of the DGLAP equations cannot be obtained in the entire range of x and Q^2, such solutions are possible under certain conditions [11, 12] and many approximated analytical solutions of DGLAP evolution equations suitable at small-x, have been reported in recent years [13-22] with considerable phenomenological success.

The singlet and non-singlet structure functions in DIS i.e. the flavor independent and flavor dependent contributions to the structure functions play the key role for accurate determination of the quark and gluon densities and therefore they can be considered as the basis for the analysis of other structure functions. In this chapter, by using a Taylor series expansion valid at small-x, we first transform the DGLAP equation, which is an integro-differential equation, into a partial differential equation in the two variables (x, Q^2) and the resulting equation is then solved at LO, NLO and NNLO respectively by the Lagrange's auxiliary method. Inclusion of the NNLO contributions considerably reduces the theoretical uncertainty of determinations of the quark and gluon densities from DIS structure functions. Here, we investigate the impact of the NNLO contributions on the evolution of the singlet and non-singlet structure function respectively considering the corresponding DGLAP evolution equations. The singlet distribution is comparatively complicated to compute as it is coupled to the the gluon densities. We also calculate the Q^2-evolution of deuteron and proton structure functions upto NNLO from the solutions of singlet and non-singlet structure functions. Moreover the x-evolution of deuteron structure function is calculated upto NNLO. We compare our predictions with NMC [23], E665 [24], and H1 [25] experimental data as well as with the NNPDF [26] parametrization based on the NMC and BCDMS data.

3.2 Formalism

3.2.1 General framework

The singlet and non-singlet quark density of a hadron is given by [27]

$$q_S(x, Q^2) = \sum_{i=1}^{N_f} [q_i(x, Q^2) + \overline{q_i}(x, Q^2)], \tag{3.1}$$

$$q_{NS}(x,Q^2) = \sum_{i=1}^{N_f}[q_i(x,Q^2) - \overline{q_i}(x,Q^2)], \tag{3.2}$$

where $q_i(x,Q^2)$ and $\overline{q_i}(x,Q^2)$ represent the number distribution of quarks and anti-quarks, respectively, in the fractional hadron momentum x. The corresponding gluon distribution is denoted by $g(x,Q^2)$. The subscript i indicates the flavour of the quarks or anti-quarks and N_f is the number of effectively massless flavours.

The DGLAP evolution equation in the singlet sector in the standard form is given by [28]

$$\frac{\partial}{\partial \ln Q^2}\begin{pmatrix} q_S \\ g \end{pmatrix} = \begin{pmatrix} P_{qq} & P_{qg} \\ P_{gq} & P_{gg} \end{pmatrix} \otimes \begin{pmatrix} q_S \\ g \end{pmatrix}, \tag{3.3}$$

where P_{qq}, P_{qg}, P_{gq}, P_{gg} are splitting functions. The singlet structure function involves the quark-quark splitting function P_{qq} and gluon-quark splitting function P_{qg}, whereas non-singlet structure function involves only the quark-quark splitting function P_{qq}. The quark-quark splitting function P_{qq} can be expressed as a power series of $\alpha_s(Q^2)$ [10]

$$\begin{aligned} P_{qq}(x,Q^2) &= \frac{\alpha_s(Q^2)}{2\pi}P_{qq}^{(0)}(x) + \Big(\frac{\alpha_s(Q^2)}{2\pi}\Big)^2 P_{qq}^{(1)}(x) + \Big(\frac{\alpha_s(Q^2)}{2\pi}\Big)^3 P_{qq}^{(2)}(x) \\ &\quad + \mathcal{O}P_{qq}^{(3)}(x), \end{aligned} \tag{3.4}$$

where $P_{qq}^{(0)}(x)$, $P_{qq}^{(1)}(x)$ and $P_{qq}^{(2)}(x)$ are LO, NLO and NNLO quark-quark splitting functions respectively. Other splitting functions can be expressed in a similar way. The symbol $\otimes$ stands for the standard Mellin Convolution in the momentum variable defined as

$$a(x) \otimes b(x) \equiv \int_x^1 \frac{d\omega}{\omega} a(\omega) b\Big(\frac{x}{\omega}\Big). \tag{3.5}$$

Thus, using Eq. (3.5), Eq. (3.3) can be written as

$$\frac{\partial}{\partial \ln Q^2}\begin{pmatrix} q_S(x,Q^2) \\ g(x,Q^2) \end{pmatrix} = \int_x^1 \frac{d\omega}{\omega}\begin{pmatrix} P_{qq}(\omega) & P_{qg}(\omega) \\ P_{gq}(\omega) & P_{gg}(\omega) \end{pmatrix}\begin{pmatrix} q_S(x/\omega,Q^2) \\ g(x/\omega,Q^2), \end{pmatrix} \tag{3.6}$$

which implies

$$\frac{\partial q_S(x,Q^2)}{\partial \ln Q^2} = \int_x^1 \frac{d\omega}{\omega}\Big(P_{qq}(\omega)q_S(x/\omega,Q^2) + P_{qg}(\omega)g(x/\omega,Q^2)\Big), \tag{3.7}$$

$$\frac{\partial g(x,Q^2)}{\partial \ln Q^2} = \int_x^1 \frac{d\omega}{\omega}\Big(P_{gq}(\omega)q_S(x/\omega,Q^2) + P_{gg}(\omega)g(x/\omega,Q^2)\Big). \tag{3.8}$$

On the other hand, the DGLAP evolution equation in the non-singlet sector in the standard form is given by [29]

$$\frac{\partial q_{NS}(x,Q^2)}{\partial \ln Q^2} = P_{NS}(x,Q^2) \otimes q_{NS}(x,Q^2), \tag{3.9}$$

where $P_{NS}(x,Q^2)$ is the non-singlet kernel known perturbatively up to the first few orders in $\alpha_s(Q^2)$ [30]. Using equation (3.5), equations (3.9) can be expressed as

$$\frac{\partial q_{NS}(x,Q^2)}{\partial \ln Q^2} = \int_x^1 \frac{d\omega}{\omega} P_{NS}(\omega) q_{NS}(x/\omega, Q^2). \tag{3.10}$$

The quark-quark splitting function P_{qq} in equation (3.6) can be expressed as $P_{qq} = P_{NS} + N_f(P_{qq}^S + P_{\bar{q}q}^S) = P_{NS} + P_{PS}$. P_{qq}^S and $P_{\bar{q}q}^S$ are the flavor-independent contributions to the quark-quark and quark-antiquark splitting functions respectively. The non-singlet contribution P_{NS} dominates P_{qq} at large-x whereas at very small-x the pure singlet term P_{PS} dominates over P_{NS} [31]. The quark-gluon (P_{qg}) and gluon-quark (P_{gq}) entries in equation (3.6) are given by $P_{qg} = N_f P_{q_i g}$ and $P_{gq} = P_{gq_i}$, where $P_{q_i g}$ and P_{gq_i} are the flavor-independent splitting functions.

The running coupling constant $\alpha_S(Q^2)$ has the form [14, 32]

$$\frac{\alpha_s(Q^2)}{2\pi} = \frac{2}{\beta_0 \ln(Q^2/\Lambda^2)}, \tag{3.11}$$

$$\frac{\alpha_s(Q^2)}{2\pi} = \frac{2}{\beta_0 \ln(Q^2/\Lambda^2)} \Big[1 - \frac{\beta_1}{\beta_0^2} \frac{\ln\big(\ln(Q^2/\Lambda^2)\big)}{\ln(Q^2/\Lambda^2)}\Big], \tag{3.12}$$

$$\begin{aligned} \frac{\alpha_s(Q^2)}{2\pi} &= \frac{2}{\beta_0 \ln(Q^2/\Lambda^2)} \Big[1 - \frac{\beta_1}{\beta_0^2} \frac{\ln\big(\ln(Q^2/\Lambda^2)\big)}{\ln(Q^2/\Lambda^2)} + \frac{1}{\beta_0^3 \ln(Q^2/\Lambda^2)} \\ &\quad \times \Big\{ \frac{\beta_1^2}{\beta_0} (\ln^2\big(\ln(Q^2/\Lambda^2)\big) - \ln\big(\ln(Q^2/\Lambda^2)\big) - 1) + \beta_2 \Big\} \Big] \end{aligned} \tag{3.13}$$

at LO, NLO and NNLO respectively. Here

$$\begin{aligned} \beta_0 &= \frac{11}{3} N_c - \frac{4}{3} T_f = 11 - \frac{2}{3} N_f, \\ \beta_1 &= \frac{34}{3} N_c^2 - \frac{10}{3} N_c N_f - 2 C_F N_f = 102 - \frac{38}{3} N_f, \\ \beta_2 &= \frac{2857}{54} N_c^3 + 2 C_F^2 T_f - \frac{205}{9} C_F N_c T_f - \frac{1415}{27} N_c^2 T_f + \frac{44}{9} C_F T_f^2 + \frac{158}{27} N_c T_f^2 \\ &= \frac{2857}{2} - \frac{6673}{18} N_f + \frac{325}{54} N_f^2 \end{aligned}$$

are the one-loop, two-loop and three-loop corrections to the QCD β-function and N_f being the number of quark flavours. Here we use $N_f = 4$, $N_c = 3$. The Casimir operators of the color $SU(3)$ are defined as $C_F = \dfrac{N_c^2 - 1}{2N_c} = \dfrac{4}{3}$ and $T_f = \dfrac{1}{2} N_f$.

3.2.2 LO analysis of singlet and non-singlet structure functions

Substituting the explicit form of the LO splitting functions [4, 11] in Eqs. (3.7) and (3.10) and simplifying, the DGLAP evolution equations for singlet and non-singlet structure functions at LO can be written as

$$\frac{\partial F_2^S(x,t)}{\partial t} = \frac{\alpha_S(t)}{2\pi}\Big[\frac{2}{3}\{3+4\ln(1-x)\}F_2^S(x,t) + I_1^S(x,t)\Big], \tag{3.14}$$

$$\frac{\partial F_2^{NS}(x,t)}{\partial t} = \frac{\alpha_S(t)}{2\pi}\Big[\frac{2}{3}\{3+4\ln(1-x)\}F_2^{NS}(x,t) + I_1^{NS}(x,t)\Big], \tag{3.15}$$

where $F_2^S(x,t) = \sum_{i=1}^{N_f} e_i^2 x[q_i + \overline{q_i}]$, and $F_2^{NS}(x,t) = \sum_{i=1}^{N_f} e_i^2 x[q_i - \overline{q_i}]]$. The integral functions are given by

$$\begin{aligned} I_1^S(x,t) &= \frac{4}{3}\int_x^1 \frac{d\omega}{1-\omega}\Big[(1+\omega^2)F_2^S\Big(\frac{x}{\omega},t\Big) - 2F_2^S(x,t)\Big] \\ &\quad + N_f\int_x^1 \{\omega^2 + (1-\omega)^2\}G\Big(\frac{x}{\omega},t\Big)d\omega, \end{aligned} \tag{3.16}$$

$$I_1^{NS}(x,t) = \frac{4}{3}\int_x^1 \frac{d\omega}{1-\omega}\Big[(1+\omega^2)F_2^{NS}\Big(\frac{x}{\omega},t\Big) - 2F_2^{NS}(x,t)\Big]. \tag{3.17}$$

Here we use a more convenient variable t defined by $t = \ln\Big(\frac{Q^2}{\Lambda^2}\Big)$ with Λ being the QCD cut off parameter, the scale at which partons turn themselves into hadrons.

To simplify and reduce the integro-differential equation to a partial differential equation we introduce a variable $u = 1-\omega$ so that the argument x/ω can be expressed as

$$\frac{x}{\omega} = \frac{x}{1-u} = x + \frac{xu}{1-u}. \tag{3.18}$$

Since $x < \omega < 1$, so we have $0 < u < 1-x$. This implies that the above series is convergent for $|u| < 1$. Now using Eq. (3.18), we can expand $F_2^S(x/\omega,t)$ by Taylor expansion series as

$$\begin{aligned} F_2^S\Big(\frac{x}{\omega},t\Big) &= F_2^S\Big(x + \frac{xu}{1-u},t\Big) \\ &= F_2^S(x,t) + \Big(\frac{xu}{1-u}\Big)\frac{\partial F_2^S(x,t)}{\partial x} + \frac{1}{2}\Big(\frac{xu}{1-u}\Big)^2\frac{\partial^2 F_2^S(x,t)}{\partial^2 x} + \cdots. \end{aligned} \tag{3.19}$$

As x is small in our region of discussion, the terms containing x^2 and higher powers of x can be neglected and therefore Eq. (3.19) takes the form

$$F_2^S\Big(\frac{x}{\omega},t\Big) = F_2^S(x,t) + \frac{xu}{1-u}\frac{\partial F_2^S(x,t)}{\partial x}. \tag{3.20}$$

Similarly,

$$G\Big(\frac{x}{\omega},t\Big) = G(x,t) + \frac{xu}{1-u}\frac{\partial G(x,t)}{\partial x}, \tag{3.21}$$

$$F_2^{NS}\Big(\frac{x}{\omega},t\Big) = F_2^{NS}(x,t) + \frac{xu}{1-u}\frac{\partial F_2^{NS}(x,t)}{\partial x}. \tag{3.22}$$

Putting Eqs. (3.20) and (3.21) in Eq. (3.16) and carrying out the integrations in u we get from Eq. (3.14)

$$\begin{aligned}\frac{\partial F_2^S(x,t)}{\partial t} &= \frac{\alpha_S(t)}{2\pi}\Big[A_1(x)F_2^S(x,t) + A_2(x)\frac{\partial F_2^S(x,t)}{\partial x} + A_3(x)G(x,t) \\ &\quad + A_4(x)\frac{\partial G(x,t)}{\partial x}\Big],\end{aligned} \tag{3.23}$$

where $A_i(x)$ (i=1,2,3,4) are functions of x (see Appendix A). Eq.(3.23) is a first order partial differential equation for the singlet structure function $F_2^S(x,t)$ with respect to the variables x and t. Beyond its traditional use in t or Q^2-evolution ($t = \ln(Q^2/\Lambda^2)$), it also provides x-evolution at small-x. There are various methods for solving the partial differential equations in two variables. We here adopt the Lagrange's auxiliary method as mentioned in the introduction.

The Q^2-evolution of the proton structure function $F_2(x,Q^2)$ is related to the gluon parton densities in the proton $G(x,Q^2)$ and to the strong interaction coupling constant α_S. The gluon parton densities cannot be measured directly through experiments. It is, therefore, important to measure the $G(x,Q^2)$ indirectly using $F_2(x,Q^2)$. Hence the direct relations between $F_2(x,Q^2)$ and the $G(x,Q^2)$ are extremely important because using those relations the experimental values of $G(x,Q^2)$ can be extracted using the data on $F_2(x,Q^2)$. Therefore, in the analytical solutions of DGLAP evolution equations for singlet structure functions or gluon parton densities, a relation between singlet structure function and gluon parton densities has to be assumed. The commonly used relation is $G(x,t) = K(x)F_2^S(x,t)$ [15, 16, 19], where $K(x)$ is a parameter to be determined from phenomenological analysis. We can consider this form as the evolution equations of gluon parton densities and singlet structure functions are in the same forms of derivative with respect to t. Moreover the input singlet and gluon parameterizations, taken from global analysis of PDFs, in particular from the MSTW08 parton set, to incorporate different high precision data, are also functions of x at fixed Q^2 [33]. So the relation between singlet structure function and gluon parton densities will come out in terms of x at fixed-Q^2. However,

the actual functional form of $K(x)$ can be determined by simultaneous solutions of coupled equations of singlet structure functions and gluon parton densities. Further discussions on $K(x)$ are presented in Appendix G.

Hence Eq.(3.23) takes the form

$$-t\frac{\partial F_2^S(x,t)}{\partial t} + L_1^S(x)\frac{\partial F_2^S(x,t)}{\partial x} + M_1^S(x)F_2^S(x,t) = 0, \tag{3.24}$$

where

$$L_1^S(x) = A_f\Big[A_2(x) + K(x)A_4(x)\Big], \tag{3.25}$$

$$M_1^S(x) = A_f\Big[A_1(x) + K(x)A_3(x) + \frac{\partial K(x)}{\partial x}A_4(x)\Big], \tag{3.26}$$

with $A_f{=}\frac{2}{\beta_0}$. Now the general solution of the Eq.(3.24) is

$$F(U,V) = 0, \tag{3.27}$$

where $F(U,V)$ is an arbitrary function of U and V. Here, $U(x,t,F_2^S) = k_1$ and $V(x,t,F_2^S) = k_2$ are two independent solutions of the Lagrange's equation

$$\frac{\partial x}{L_1^S(x)} = \frac{\partial t}{-t} = \frac{\partial F_2^S(x,t)}{-M_1^S(x)F_2^S(x,t)}. \tag{3.28}$$

Then by solving Eq. (3.28) we obtain

$$U(x,t,F_2^S) = t\cdot\exp\Big[\int\frac{1}{L_1^S(x)}dx\Big], \tag{3.29}$$

$$V(x,t,F_2^S) = F_2^S(x,t)\cdot\exp\Big[\int\frac{M_1^S(x)}{L_1^S(x)}dx\Big]. \tag{3.30}$$

Thus we see that it has no unique solution. In this approach we attempt to extract a particular solution that obeys some physical constraints on the structure function. The simplest possibility to get a solution is that a linear combination of U and V should obey the Eq. (3.27) so that

$$\alpha\cdot U + \beta\cdot V = 0, \tag{3.31}$$

where α and β are arbitrary constants to be determined from the boundary conditions on F_2^S. Putting the values of U and V from Eq.(3.29) and Eq.(3.30) in this equation we get

$$\alpha t\cdot\exp\Big[\int\frac{1}{L_1^S(x)}dx\Big] + \beta F_2^S(x,t)\cdot\exp\Big[\int\frac{M_1^S(x)}{L_1^S(x)}dx\Big] = 0, \tag{3.32}$$

which implies

$$F_2^S(x,t) = -\gamma t \cdot \exp\Big[\int \big(\frac{1}{L_1^S(x)} - \frac{M_1^S(x)}{L_1^S(x)}\big)dx\Big], \tag{3.33}$$

where $\gamma = \frac{\alpha}{\beta}$ is a constant. Now at $t = t_0$, where $t_0 = \ln\Big(\frac{Q_0^2}{\Lambda^2}\Big)$ for any lower value $Q^2 = Q_0^2$, we define

$$F_2^S(x,t_0) = -\gamma t_0 \cdot \exp\Big[\int \big(\frac{1}{L_1^S(x)} - \frac{M_1^S(x)}{L_1^S(x)}\big)dx\Big]. \tag{3.34}$$

Then Eqs. (3.33) and (3.34) lead us to

$$F_2^S(x,t) = F_2^S(x,t_0)\Big(\frac{t}{t_0}\Big). \tag{3.35}$$

This gives the t-evolution for singlet structure function at LO at small-x. Again defining at a higher value of $x = x_0$,

$$F_2^S(x_0,t) = -\gamma t \cdot \exp\Big[\int \big(\frac{1}{L_1^S(x)} - \frac{M_1^S(x)}{L_1^S(x)}\big)dx\Big]_{x=x_0}, \tag{3.36}$$

we obtain

$$F_2^S(x,t) = F_2^S(x_0,t) \cdot \exp\Big[\int_{x_0}^{x} \big(\frac{1}{L_1^S(x)} - \frac{M_1^S(x)}{L_1^S(x)}\big)dx\Big]. \tag{3.37}$$

This gives the x-evolutions of singlet structure functions at LO.

Now substituting the approximated form of Taylor expansion of non-singlet structure function from Eq.(3.22) in Eq.(3.17) and performing u-integrations we obtain from Eq.(3.15)

$$\frac{\partial F_2^{NS}(x,t)}{\partial t} = \frac{\alpha_S(t)}{2\pi}\Big[A_1(x)F_2^{NS}(x,t) + A_2(x)\frac{\partial F_2^{NS}(x,t)}{\partial x}\Big], \tag{3.38}$$

which we can rewrite as

$$-t\frac{\partial F_2^{NS}(x,t)}{\partial t} + L_1^{NS}(x)\frac{\partial F_2^{NS}(x,t)}{\partial x} + M_1^{NS}(x)F_2^{NS}(x,t) = 0. \tag{3.39}$$

Here

$$L_1^{NS}(x) = A_f A_2(x), \tag{3.40}$$

$$M_1^{NS}(x) = A_f A_1(x). \tag{3.41}$$

Proceeding in the same way as the singlet case we solve Eq. (3.39) for non-singlet structure function and obtain

$$F_2^{NS}(x,t) = F_2^{NS}(x,t_0)\Big(\frac{t}{t_0}\Big) \tag{3.42}$$

and

$$F_2^{NS}(x,t) = F_2^{NS}(x_0,t) \cdot \exp\Big[\int_{x_0}^{x} \big(\frac{1}{L_1^{NS}(x)} - \frac{M_1^{NS}(x)}{L_1^{NS}(x)}\big)dx\Big], \tag{3.43}$$

which give the t and x-evolutions of non-singlet structure functions respectively at LO respectively.

For phenomenological analysis, we compare our results with various experimental structure functions. The deuteron structure function measured in DIS can be written in terms of the singlet structure function respectively as [11]

$$F_2^d(x,t) = \frac{5}{9}F_2^S(x,t). \tag{3.44}$$

Again the proton structure function measured in DIS can be expressed in terms of the singlet and non-singlet structure function as [11]

$$F_2^p(x,t) = \frac{5}{18}F_2^S(x,t) + \frac{3}{18}F_2^{NS}(x,t). \tag{3.45}$$

Substituting Eqs. (3.35) and (3.37) in Eq. (3.44), the t and x-evolutions of deuteron structure function at LO can be obtained as

$$F_2^d(x,t) = F_2^d(x,t_0)\Big(\frac{t}{t_0}\Big) \tag{3.46}$$

and

$$F_2^d(x,t) = F_2^d(x_0,t) \cdot \exp\Big[\int_{x_0}^{x} \big(\frac{1}{\overline{L_1^S}(x)} - \frac{\overline{M_1^S}(x)}{\overline{L_1^S}(x)}\big)dx\Big]. \tag{3.47}$$

Here the input functions are $F_2^d(x,t_0) = \frac{5}{9}F_2^S(x,t_0)$ and $F_2^d(x_0,t) = \frac{5}{9}F_2^S(x_0,t)$.

On the other hand, substituting Eqs. (3.35) and (3.42) in Eq. (3.45), we get the t-evolutions of proton structure function at LO

$$F_2^p(x,t) = F_2^p(x,t_0)\Big(\frac{t}{t_0}\Big), \tag{3.48}$$

with the input function is $F_2^p(x,t_0) = \frac{5}{18}F_2^S(x,t_0) + \frac{3}{18}F_2^{NS}(x,t_0)$. It is to be noted that the determination of x-evolution of proton structure function like that of deuteron structure function is not suitable by the method adopted here. The reason is that in order to calculate the x-evolution of proton structure function, we have to put Eqs. (3.37) and (3.43) in Eq. (3.45). But the functions inside the integral sign of Eqs. (3.37) and (3.43) are different and so the the input functions $F_2^S(x_0,t)$ and $F_2^{NS}(x_0,t)$ have to be separated from the data points to extract the x-evolution of the proton function, which may contain large errors.

3.2.3 NLO analysis of singlet and non-singlet structure functions

Considering the splitting functions at NLO [12, 34, 35], the DGLAP equations for singlet and non-singlet structure functions at NLO in standard form can be written as

$$\begin{aligned}\frac{\partial F_2^S(x,t)}{\partial t} &= \frac{\alpha_S(t)}{2\pi}\Big[\frac{2}{3}\{3+4\ln(1-x)\}F_2^S(x,t)+I_1^S(x,t)\Big] \\ &\quad+\Big(\frac{\alpha_S(t)}{2\pi}\Big)^2 I_2^S(x,t), \end{aligned} \tag{3.49}$$

$$\begin{aligned}\frac{\partial F_2^{NS}(x,t)}{\partial t} &= \frac{\alpha_S(t)}{2\pi}\Big[\frac{2}{3}\{3+4\ln(1-x)\}F_2^{NS}(x,t)+I_1^{NS}(x,t)\Big] \\ &\quad+\Big(\frac{\alpha_S(t)}{2\pi}\Big)^2 I_2^{NS}(x,t). \end{aligned} \tag{3.50}$$

The integral functions $I_1^S(x,t)$ and $I_1^{NS}(x,t)$ are defined in Eqs. (3.16) and (3.17), whereas

$$\begin{aligned}I_2^S(x,t) &= (x-1)F_2^S(x,t)\int_0^1 f(\omega)d\omega+\int_x^1 f(\omega)F_2^S\Big(\frac{x}{\omega},t\Big)d\omega \\ &\quad+\int_x^1 F_{qq}^S(\omega)F_2^S\Big(\frac{x}{\omega},t\Big)d\omega+\int_x^1 F_{qg}^S(\omega)G\Big(\frac{x}{\omega},t\Big)d\omega, \end{aligned} \tag{3.51}$$

$$I_2^{NS}(x,t)=(x-1)F_2^{NS}(x,t)\int_0^1 f(\omega)d\omega+\int_x^1 f(\omega)F_2^{NS}\Big(\frac{x}{\omega},t\Big)d\omega. \tag{3.52}$$

The explicit forms of the functions $f(\omega)$, $F_{qq}^S(\omega)$ and $F_{qg}^S(\omega)$ are given in Appendix B.

Following the same procedure as in LO, the Eqs. (3.49) and (3.50) can be simplified as

$$-t\frac{\partial F_2^S(x,t)}{\partial t}+L_2^S(x)\frac{\partial F_2^S(x,t)}{\partial x}+M_2^S(x)F_2^S(x,t)=0, \tag{3.53}$$

$$-t\frac{\partial F_2^{NS}(x,t)}{\partial t}+L_2^{NS}(x)\frac{\partial F_2^{NS}(x,t)}{\partial x}+M_2^{NS}(x)F_2^{NS}(x,t)=0. \tag{3.54}$$

Here

$$L_2^S(x)=A_f\Big[\Big(A_2(x)+K(x)A_4(x)\Big)+T_0\Big(B_2(x)+K(x)B_4(x)\Big)\Big], \tag{3.55}$$

$$\begin{aligned}M_2^S(x) &= A_f\Big[\Big(A_1(x)+K(x)A_3(x)+\frac{\partial K(x)}{\partial x}A_4(x)\Big) \\ &\quad+T_0\Big(B_1(x)+K(x)B_3(x)+\frac{\partial K(x)}{\partial x}B_4(x)\Big)\Big], \end{aligned} \tag{3.56}$$

$$L_2^{NS}(x) = A_f\Big[A_2(x) + T_0 B_2(x)\Big], \tag{3.57}$$

$$M_2^{NS}(x) = A_f\Big[A_1(x) + T_0 B_1(x)\Big], \tag{3.58}$$

with $B_i(x)$ (i=1,2,3,4) being the functions of x (see Appendix A). Here we consider the numerical parameter T_0 such that $T^2(t) = T_0 T(t)$ where $T(t)=\frac{\alpha_S(t)}{2\pi}$ and the value of T_0 is determined by phenomenological analysis. This numerical parameter is obtained from a particular range of Q^2 under study and by a suitable choice of T_0 we can reduce the difference between $T^2(t)$ and $T_0 T(t)$ to a minimum. Thus the consideration of the parameter T_0 does not give any abrupt change in our result.

Solving Eq. (3.53) we obtain the t and x-evolutions of singlet structure function at NLO as

$$F_2^S(x,t) = F_2^S(x,t_0)\Big(\frac{t^{1+b/t}}{t_0^{1+b/t_0}}\Big)\cdot\exp\Big(\frac{b}{t}-\frac{b}{t_0}\Big) \tag{3.59}$$

and

$$F_2^S(x,t) = F_2^S(x_0,t)\cdot\exp\Big[\int_{x_0}^{x}\big(\frac{1}{L_2^S(x)}-\frac{M_2^S(x)}{L_2^S(x)}\big)dx\Big], \tag{3.60}$$

where $b=\frac{\beta_1}{\beta_0^2}$. The input functions are defined as

$$F_2^S(x,t_0) = -\gamma t_0^{(1+b/t_0)}\cdot\exp\Big(\frac{b}{t_0}\Big)\cdot\exp\Big[\int\big(\frac{1}{L_2^S(x)}-\frac{M_2^S(x)}{L_2^S(x)}\big)dx\Big], \tag{3.61}$$

$$F_2^S(x_0,t) = -\gamma t^{(1+b/t)}\cdot\exp\Big(\frac{b}{t}\Big)\cdot\exp\Big[\int\big(\frac{1}{L_2^S(x)}-\frac{M_2^S(x)}{L_2^S(x)}\big)dx\Big]_{x=x_0}. \tag{3.62}$$

Now substituting Eqs. (3.59) and (3.60) in Eq. (3.44) we get

$$F_2^d(x,t) = F_2^d(x,t_0)\Big(\frac{t^{1+b/t}}{t_0^{1+b/t_0}}\Big)\cdot\exp\Big(\frac{b}{t}-\frac{b}{t_0}\Big) \tag{3.63}$$

and

$$F_2^d(x,t) = F_2^d(x_0,t)\cdot\exp\Big[\int_{x_0}^{x}\big(\frac{1}{L_2^S(x)}-\frac{M_2^S(x)}{L_2^S(x)}\big)dx\Big], \tag{3.64}$$

which lead us to the t and x-evolutions of deuteron structure function at NLO.

Similarly the t and x-evolutions of the non-singlet structure function at NLO are calculated from Eq. (3.54) and given by

$$F_2^{NS}(x,t) = F_2^{NS}(x,t_0)\Big(\frac{t^{1+b/t}}{t_0^{1+b/t_0}}\Big)\cdot\exp\Big(\frac{b}{t}-\frac{b}{t_0}\Big) \tag{3.65}$$

and

$$F_2^{NS}(x,t) = F_2^{NS}(x_0,t)\cdot\exp\Big[\int_{x_0}^{x}\big(\frac{1}{L_2^{NS}(x)} - \frac{M_2^{NS}(x)}{L_2^{NS}(x)}\big)dx\Big]. \tag{3.66}$$

Thus putting Eqs. (3.59) and (3.65) in Eq. (3.45) we get

$$F_2^{p}(x,t) = F_2^{p}(x,t_0)\Big(\frac{t^{1+b/t}}{t_0^{1+b/t_0}}\Big)\cdot\exp\Big(\frac{b}{t}-\frac{b}{t_0}\Big), \tag{3.67}$$

which lead us to the t-evolution of proton structure function at NLO. It is not possible to evaluate the x-evolution of proton structure function with the present method for the same reason mentioned earlier.

3.2.4 NNLO analysis of singlet and non-singlet structure functions

Using the splitting functions upto NNLO and simplifying [28-31], we get the DGLAP equations for singlet and non-singlet structure functions at NNLO as

$$\begin{aligned}\frac{\partial F_2^S(x,t)}{\partial t} &= \frac{\alpha_S(t)}{2\pi}\Big[\frac{2}{3}\{3+4\ln(1-x)\}F_2^S(x,t)+I_1^S(x,t)\Big]\\ &\quad+\Big(\frac{\alpha_S(t)}{2\pi}\Big)^2 I_2^S(x,t)+\Big(\frac{\alpha_S(t)}{2\pi}\Big)^3 I_3^S(x,t),\end{aligned} \tag{3.68}$$

$$\begin{aligned}\frac{\partial F_2^{NS}(x,t)}{\partial t} &= \frac{\alpha_S(t)}{2\pi}\Big[\frac{2}{3}\{3+4\ln(1-x)\}F_2^{NS}(x,t)+I_1^{NS}(x,t)\Big]\\ &\quad+\Big(\frac{\alpha_S(t)}{2\pi}\Big)^2 I_2^{NS}(x,t)+\Big(\frac{\alpha_S(t)}{2\pi}\Big)^3 I_3^{NS}(x,t).\end{aligned} \tag{3.69}$$

The integral functions I_3^S and I_3^{NS} are given by

$$I_3^S(x,t) = \int_x^1\frac{d\omega}{\omega}\Big[P_{qq}(x)F_2^S\Big(\frac{x}{\omega},t\Big)+P_{qg}(x)G\Big(\frac{x}{\omega},t\Big)\Big], \tag{3.70}$$

$$I_3^{NS}(x,t) = \int_x^1\frac{d\omega}{\omega}P_{NS}^2(x)F_2^{NS}\Big(\frac{x}{\omega},t\Big). \tag{3.71}$$

The explicit forms of the functions $P_{qq}(x)$, $P_{qg}(x)$ and $P_{NS}^2(x)$ are given in Appendix C.

Here we consider the numerical parameter T_1 such that $T^3(t) = T_1T(t)$ where $T(t)$=$\frac{\alpha_S(t)}{2\pi}$. The value of T_1 is determined by phenomenological analysis, like T_0, from a particular range of Q^2 under study and by an appropriate choice of T_1 we can reduce the error to a minimum. Thus Eqs. (3.68) and (3.69) can be simplified as

$$-t\frac{\partial F_2^S(x,t)}{\partial t}+L_3^S(x)\frac{\partial F_2^S(x,t)}{\partial x}+M_3^S(x)F_2^S(x,t)=0, \tag{3.72}$$

$$-t\frac{\partial F_2^{NS}(x,t)}{\partial t} + L_3^{NS}(x)\frac{\partial F_2^{NS}(x,t)}{\partial x} + M_3^{NS}(x)F_2^{NS}(x,t) = 0. \tag{3.73}$$

Here

$$\begin{aligned} L_3^S(x) &= A_f\Big[\Big(A_2(x) + K(x)A_4(x)\Big) + T_0\Big(B_2(x) + K(x)B_4(x)\Big) \\ &\quad + T_1\Big(C_2(x) + K(x)C_4(x)\Big)\Big], \end{aligned} \tag{3.74}$$

$$\begin{aligned} M_3^S(x) &= A_f\Big[\Big(A_1(x) + K(x)A_3(x) + \frac{\partial K(x)}{\partial x}A_4(x)\Big) + T_0\Big(B_1(x) \\ &\quad + K(x)B_3(x) + \frac{\partial K(x)}{\partial x}B_4(x)\Big) + T_1\Big(C_1(x) + K(x)C_3(x) \\ &\quad + \frac{\partial K(x)}{\partial x}C_4(x)\Big)\Big], \end{aligned} \tag{3.75}$$

$$L_3^{NS}(x) = A_f\Big[A_2(x) + T_0B_2(x) + T_1C_2(x)\Big], \tag{3.76}$$

$$M_2^{NS}(x) = A_f\Big[A_1(x) + T_0B_1(x) + T_1C_1(x)\Big] \tag{3.77}$$

with $C_i(x)$ (i=1,2,3,4) being the functions of x (see Appendix A).

We solve Eq. (3.72) following the same procedure as earlier and obtain the t and x-evolutions of singlet structure function at NNLO given by

$$F_2^S(x,t) = F_2^S(x,t_0)\Big(\frac{t^{1+(b-b^2)/t}}{t_0^{1+(b-b^2)/t_0}}\Big)\cdot\exp\Big(\frac{b-c-b^2\ln^2 t}{t} - \frac{b-c-b^2\ln^2 t_0}{t_0}\Big) \tag{3.78}$$

and

$$F_2^S(x,t) = F_2^S(x_0,t)\cdot\exp\Big[\int_{x_0}^{x}\big(\frac{1}{L_3^S(x)} - \frac{M_3^S(x)}{L_3^S(x)}\big)dx\Big] \tag{3.79}$$

respectively. The input functions are defined as

$$\begin{aligned} F_2^S(x,t_0) &= -\gamma t_0^{(1+(b-b^2)/t_0)}\cdot\exp\Big(\frac{b-c-b^2\ln^2 t_0}{t_0}\Big)\cdot\exp\Big[\int\big(\frac{1}{L_3^S(x)} \\ &\quad - \frac{M_3^S(x)}{L_3^S(x)}\big)dx\Big], \end{aligned} \tag{3.80}$$

$$\begin{aligned} F_2^S(x_0,t) &= -\gamma t^{(1+(b-b^2)/t)}\cdot\exp\Big(\frac{b-c-b^2\ln^2 t}{t}\Big)\cdot\exp\Big[\int\big(\frac{1}{L_3^S(x)} \\ &\quad - \frac{M_3^S(x)}{L_3^S(x)}\big)dx\Big]_{x=x_0} \end{aligned} \tag{3.81}$$

with $b = \frac{\beta_1}{\beta_0^2}, c = \frac{\beta_2}{\beta_0^3}$. Accordingly substituting Eqs. (3.78) and (3.79) in Eq. (3.44) we get

$$F_2^d(x,t) = F_2^d(x,t_0)\Big(\frac{t^{1+(b-b^2)/t}}{t_0^{1+(b-b^2)/t_0}}\Big)\cdot\exp\Big(\frac{b-c-b^2\ln^2 t}{t}-\frac{b-c-b^2\ln^2 t_0}{t_0}\Big) \tag{3.82}$$

and

$$F_2^d(x,t) = F_2^d(x_0,t)\cdot\exp\Big[\int_{x_0}^{x}\big(\frac{1}{L_3^S(x)}-\frac{M_3^S(x)}{L_3^S(x)}\big)dx\Big], \tag{3.83}$$

which provide us the t and x-evolutions of deuteron structure functions at NNLO. Thus using Eq.(3.82) we can calculate the evolution of deuteron structure function with t or Q^2 at fixed x at NNLO by choosing an appropriate input distribution $F_2^d(x,t_0)$ at $Q^2 = Q_0^2$. Similarly Eq.(3.83) helps us to estimate the x-evolution of deuteron structure function at fixed t or Q^2 with a suitable input distribution $F_2^d(x_0,t)$ at a given value $x = x_0$.

Similarly, the solution of (3.73) provide us the t and x-evolutions of the non-singlet structure function given by

$$F_2^{NS}(x,t) = F_2^{NS}(x,t_0)\Big(\frac{t^{1+(b-b^2)/t}}{t_0^{1+(b-b^2)/t_0}}\Big)\cdot\exp\Big(\frac{b-c-b^2\ln^2 t}{t}-\frac{b-c-b^2\ln^2 t_0}{t_0}\Big) \tag{3.84}$$

and

$$F_2^{NS}(x,t) = F_2^{NS}(x_0,t)\cdot\exp\Big[\int_{x_0}^{x}\big(\frac{1}{L_3^{NS}(x)}-\frac{M_3^{NS}(x)}{L_3^{NS}(x)}\big)dx\Big] \tag{3.85}$$

respectively. The input functions are defined as

$$\begin{aligned} F_2^{NS}(x,t_0) &= -\gamma t_0^{(1+(b-b^2)/t_0)}\cdot\exp\Big(\frac{b-c-b^2\ln^2 t_0}{t_0}\Big)\cdot\exp\Big[\int\big(\frac{1}{L_3^{NS}(x)} \\ &\quad -\frac{M_3^{NS}(x)}{L_3^{NS}(x)}\big)dx\Big], \end{aligned} \tag{3.86}$$

$$\begin{aligned} F_2^{NS}(x_0,t) &= -\gamma t^{(1+(b-b^2)/t)}\cdot\exp\Big(\frac{b-c-b^2\ln^2 t}{t}\Big)\cdot\exp\Big[\int\big(\frac{1}{L_3^{NS}(x)} \\ &\quad -\frac{M_3^{NS}(x)}{L_3^{NS}(x)}\big)dx\Big]_{x=x_0}. \end{aligned} \tag{3.87}$$

Thus putting Eq.(3.78) and Eq. (3.84) in Eq.(3.45) we obtain

$$F_2^p(x,t) = F_2^p(x,t_0)\Big(\frac{t^{1+(b-b^2)/t}}{t_0^{1+(b-b^2)/t_0}}\Big)\cdot\exp\Big(\frac{b-c-b^2\ln^2 t}{t}-\frac{b-c-b^2\ln^2 t_0}{t_0}\Big), \tag{3.88}$$

which gives the t-evolution of proton structure function. By considering a suitable input distribution $F_2^p(x,t_0)$ at a given value $Q^2 = Q_0^2$, we can determine the evolution of proton structure function with t or Q^2 at some fixed x from Eq.(3.88). The x evolution of proton structure function is not possible at NNLO for the same reason discussed earlier.

For phenomenological analysis of t-evolution, we take the input distributions $F_2^d(x,t_0)$ and $F_2^p(x,t_0)$ from experimental data corresponding to the lowest value of the Q^2 range considered in our study. Similarly the input functions $F_2^d(x_0,t)$ for phenomenological analysis of x-evolution are taken from the experimental data corresponding to the highest value of the x range under consideration.

3.3 Result and discussion

In this chapter, we calculate the Q^2 or t ($t = \ln(Q^2/\Lambda^2)$) and x-evolutions of singlet and non-singlet structure functions. The deuteron and proton structure functions are related to the singlet and non-singlet structure functions as given by the Eqs. (3.48) and (3.49). We calculate the t and x-evolutions of deuteron stucture function at LO, NLO and NNLO respectively. The t-evolution of proton structure function is also obtained up to NNLO. We test the validity of the solutions, by comparing them directly with the available data on deuteron and proton structure function. For our analysis we use the data from the fixed target experiments viz. the NMC [23] in muon-deuteron DIS from the merged data sets at incident momenta 90, 120, 200 and 280 GeV^2, the Fermilab E665 [24] collaboration in muon-deuteron DIS at an average beam energy of 470 GeV^2 and the H1 collaboration of HERA experiment data [25] taken with a 26.7 GeV electron beam in collision with a 820 GeV proton beam. We consider the H1 1995 data because these data sets are available in the range of our consideration. Moreover, we compare our results with those obtained by the fit to F_2^d produced by the NNPDF parametrization [26]. The NNPDF parametrization presents a determination of the probability density in the space of F_2 structure functions for the proton, deuteron and non-singlet structure function, as determined from experimental data of NMC [23], E665 [24], BCDMS [36] and H1 [37] collaborations. Their results take the form of a set of 1000 neural nets, for each of the three structure functions, which give a determination of F_2 for given x and Q^2. The central value and

the errors of the structure functions determined in the NNPDF fit can be computed out of the ensemble of 1000 nets according to standard Monte Carlo techniques. We consider the range $0.0045 \leq x \leq 0.19$ and $0.75 \leq Q^2 \leq 27$ GeV^2 for NMC data, $0.0052 \leq x \leq 0.18$ and $1.094 \leq Q^2 \leq 26$ GeV^2 for E665 data and $0.004 \leq x \leq 0.03$ and $5.5 \leq Q^2 \leq 38$ GeV^2 for H1 data for our phenomenological analysis. Similarly we use the range $0.0045 \leq x \leq 0.095$ and $1.25 \leq Q^2 \leq 26$ GeV^2 to compare our results with the NNPDF parametrization. For the fit we consider $\Lambda_{\overline{MS}} = 323$ MeV for $\alpha_s(M_z^2) = 0.119 \pm 0.002$. The vertical error bars represent the total combined statistical and systematic uncertainties of the experimental data. To compute the dependence of structure functions on Q^2 or in other words for t-evolution, we take the input distributions from the data point corresponding to the lowest value of Q^2 for a particular range of Q^2 under study. Similarly the data point corresponding to the highest value of x of a particular range of x under consideration are taken as input distribution to determine the x dependence of the structure functions.

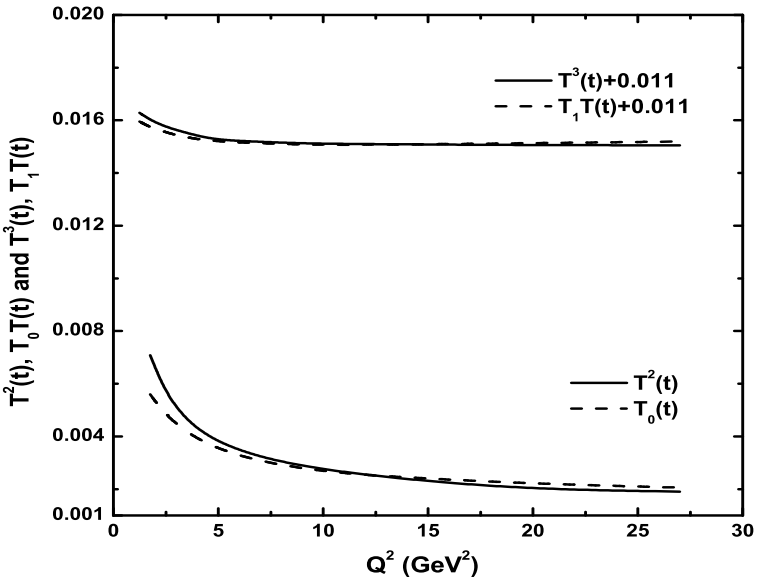

Figure 3.1: Comparison of T^2 and $T_0.T(t)$ as well as T^3 and $T_1.T(t)$ versus Q^2.

As mentioned earlier for the analytical solution of DGLAP evolution equation for singlet structure function we consider a function $K(x)$ which relates the singlet structure function and gluon densities. For simplicity we consider the function $K(x) = K$, where K is an arbitrary constant parameter. We examine the dependence of our predictions on the values of the arbitrary constant K and find that the best fit results

are obtained in the range $0.45 < K < 1.6$ for our entire region of discussion.

As discussed in section 3.2 the numerical parameters T_0 and T_1, considered for the solutions of the DGLAP equations at NLO and NNLO respectively, are obtained for a particular domain of Q^2 under study. To this end in Figure 3.1 we plot $T^2(t)$ and $T_0T(t)$ as well as $T^3(t)$ and $T_1T(t)$ as a function of Q^2. We find that for $T_0 = 0.048$ the difference between $T^2(t)$ and $T_0T(t)$ is reduced to a minimum and for $T_1 = 0.008$ the difference between $T^3(t)$ and $T_1T(t)$ becomes negligible in the range $0.75 < Q^2 < 50$ GeV^2. Therefore the consideration of the parameters T_0 and T_1 does not induce any unexpected change in our results.

In Figure 3.2 we plot the predictions of the deuteron structure function obtained from Eqs.(3.46), (3.63) and (3.82) for LO, NLO and NNLO respectively as functions of Q^2 at four representative values $x = 0.0045, 0.0125, 0.0175$ and 0.025 respectively. Here we compare our results with the NMC experimental data in the range $0.75 \leq Q^2 \leq 27$ GeV^2.

In Figure 3.3 we plot our our set of solutions Eqs. (3.47), (3.64) and (3.83) for deuteron structure function at LO, NLO and NNLO respectively as functions of x for four fixed $Q^2 = 7, 11.5, 20$ and 27 GeV^2 respectively. Our predictions are compared with the NMC experimental data in the range $0.0045 \leq x \leq 0.19$.

Figure 3.4 represent the comparison of our results of t or Q^2 evolution of deuteron structure function calculated from Eqs.(3.46), (3.63) and (3.82) for LO, NLO and NNLO respectively with the E665 experimental data. Here we plot our predictions of deuteron structure function as functions of Q^2 considering the range $1.094 \leq Q^2 \leq 26$ GeV^2 at fixed values of x, viz. $x = 0.0052, 0.00893, 0.0125$ and 0.0173 respectively.

In Figure 3.5 we plot our computed results of deuteron structure function obtained from Eqs.(3.47), (3.64) and (3.83) for LO, NLO and NNLO respectively as functions of x and compare with the E665 experimental data considering the range $0.0052 \leq x \leq 0.18$. The comparison is shown for four fixed $Q^2 = 5.236, 9.795, 18.323$ and 25.061 GeV^2 respectively.

Figure 3.6 shows the Q^2 evolution of deuteron structure function obtained from Eqs.(3.46), (3.63) and (3.82) at LO, NLO and NNLO respectively compared with the NNPDF parametrization in the range $1.25 \leq Q^2 \leq 26$ GeV^2. We perform the comparison for four different values of x, x=0.0045, 0.008, 0.0125 and 0.0175

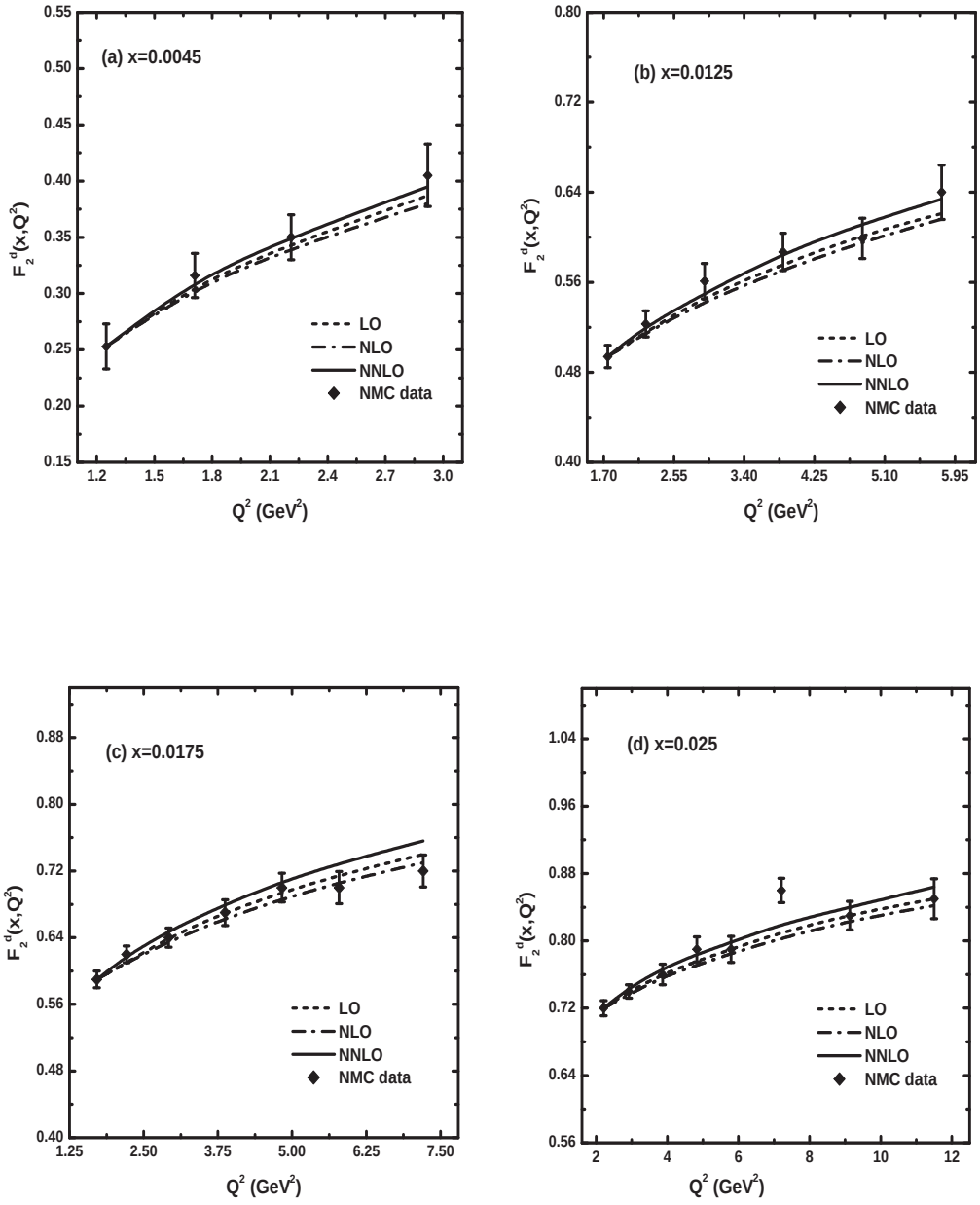

Figure 3.2: Comparison of Q^2 evolution of deuteron structure functions at LO, NLO and NNLO with the NMC data for four fixed values x. The dot lines represent the LO results (Eq.3.46), dash-dot lines represent the NLO results (Eq.3.63) and solid lines represent the NNLO results Eq.(3.82).

respectively.

In Figure 3.7 show the comparison of our results of x-evolutions of deuteron structure function obtained from Eqs.(3.47), (3.64) and (3.83) at LO, NLO and NNLO with those obtained by the NNPDF parametrization in the range $0.0045 \leq x \leq 0.095$. The comparison is done for four fixed values of Q^2 viz. $Q^2 = 5, 9, 15$ and 25 GeV^2

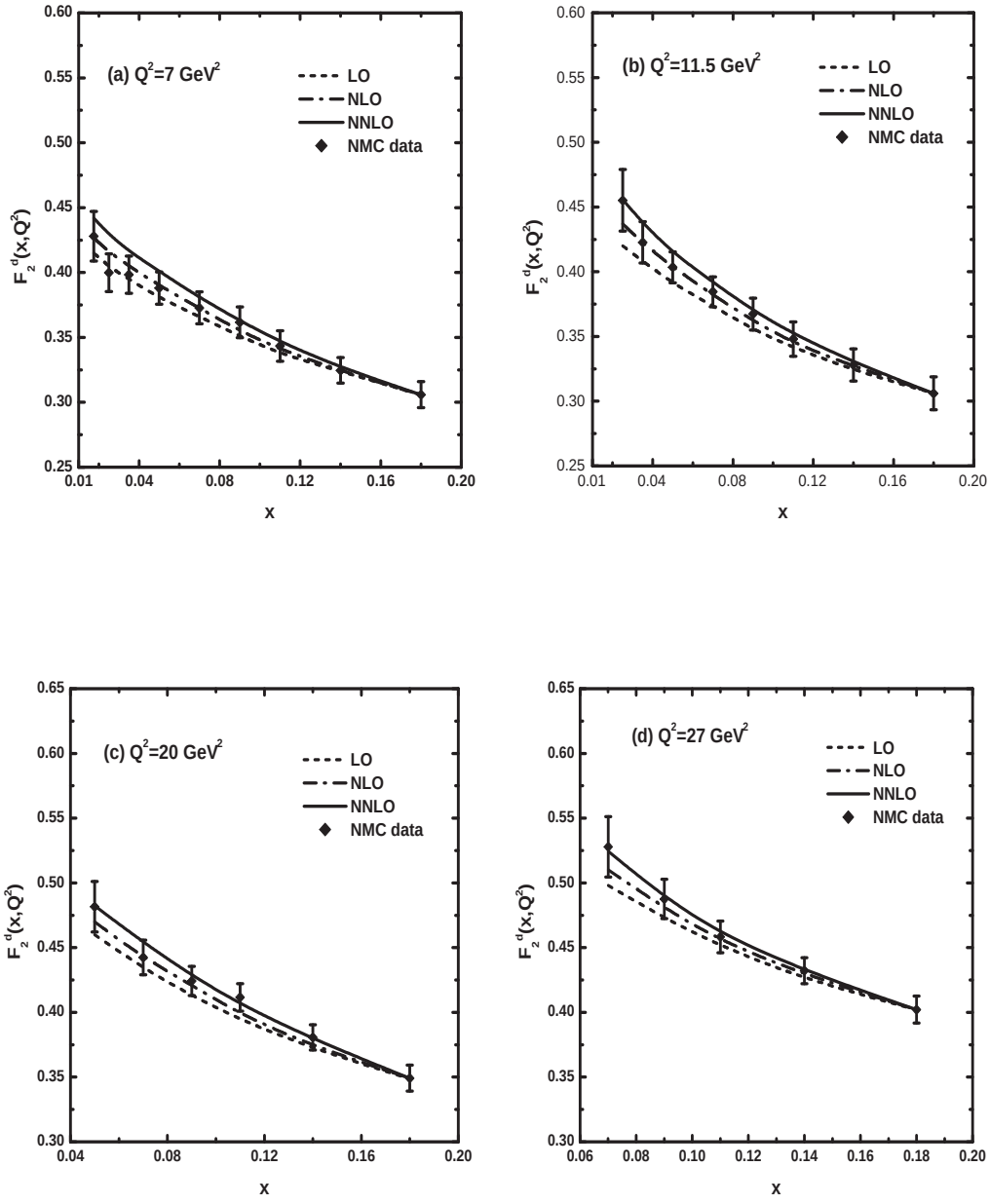

Figure 3.3: Plots of x evolution of deuteron structure function at LO, NLO and NNLO compared with the NMC data for four fixed Q^2. The dot lines represent the LO results (Eq.3.47), dash-dot lines represent the NLO results (Eq.3.64) and solid lines represent the NNLO results Eq.(3.83).

respectively.

We also calculate the t or Q^2-evolution of proton structure function at LO, NLO and NNLO from Eq. (3.48), (3.67) and (3.88). Figure 3.8 show the comparison of our results of proton structure function with those measured at NMC as functions of Q^2 in the range $0.75 \leq Q^2 \leq 27$ GeV^2. We show the comparison for four fixed $x = 0.008, 0.0125, 0.025$ and 0.035 respectively.

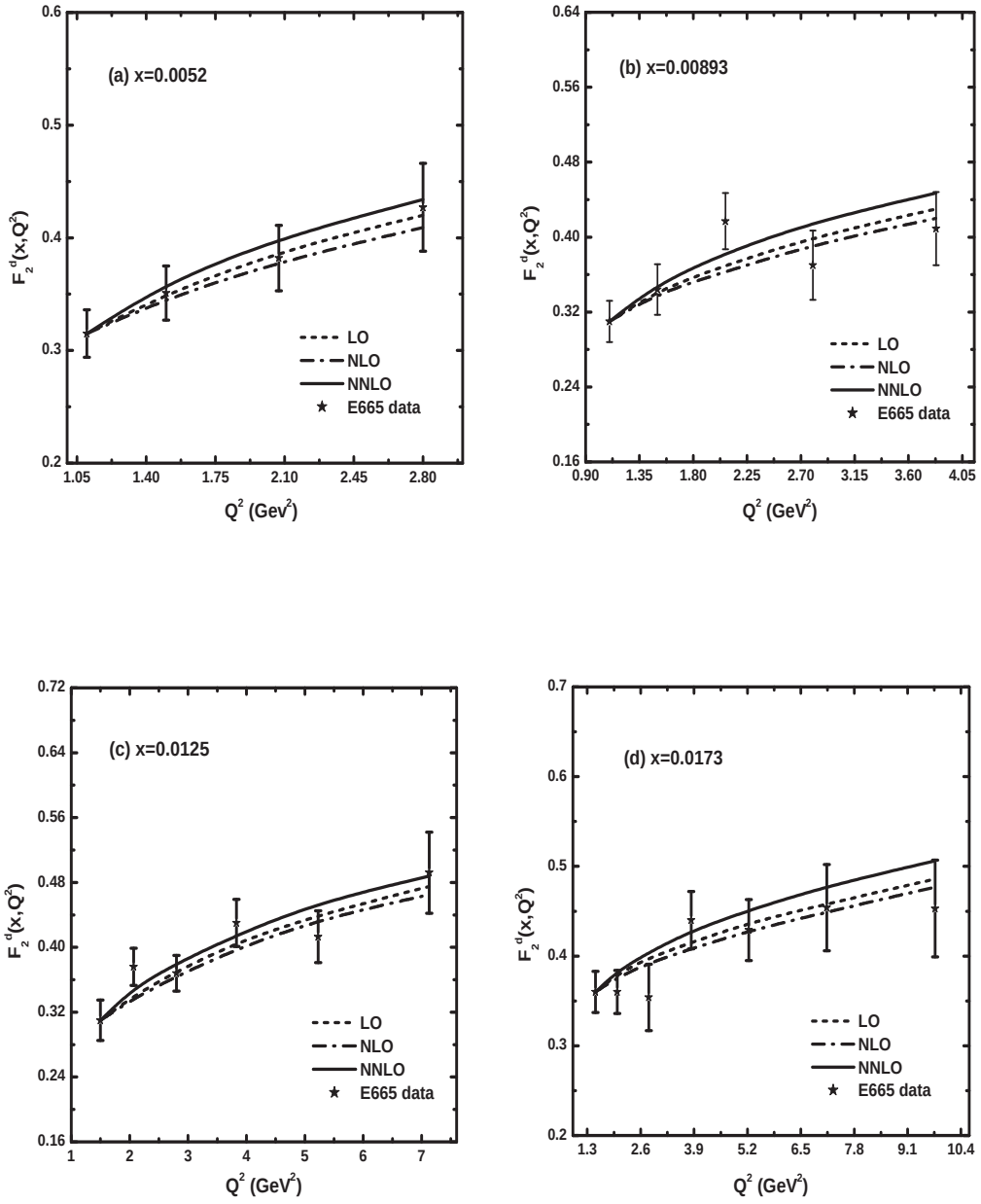

Figure 3.4: Plots of Q^2 evolution of deuteron structure functions at LO, NLO and NNLO compared with the E665 data for four representative x. The dot lines are the LO results (Eq.3.46), dash-dot lines are the NLO results (Eq.3.63) and solid lines are the NNLO results (Eq.3.82).

Figure 3.9 show the comparison of our solution of proton structure function given by Eqs.(3.48), (3.67) and (3.88) for LO, NLO and NNLO respectively with the E665 experimental data in the range $1.094 \leq Q^2 \leq 26$ GeV^2. Here we plot the computed values of proton structure function as functions of Q^2 at four representative values of x, namely $x = 0.00693, 0.01225, 0.0173$ and 0.02449 respectively.

In Figure 3.10 we plot our computed results of proton structure function ob-

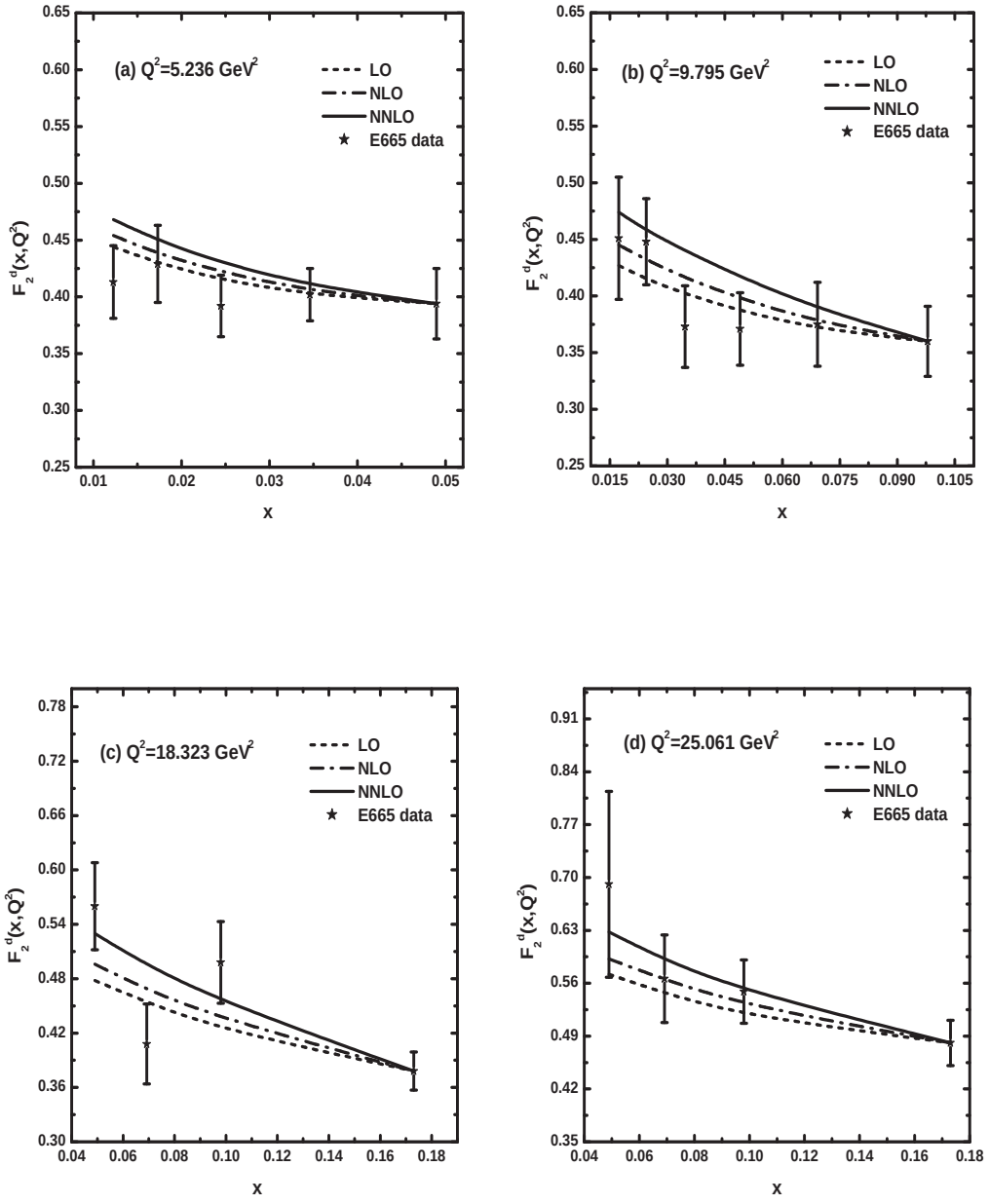

Figure 3.5: Comparison of x evolution of deuteron structure function at LO, NLO and NNLO with the E665 data for four representative values of Q^2 . The dot lines represent the LO results (Eq.3.47), dash-dot lines represent the NLO results (Eq.3.64) and solid lines represent the NNLO results Eq.(3.83).

tained from Eqs.(3.48), (3.67) and (3.88) for LO, NLO and NNLO respectively as functions of Q^2 and compare with the H1 1995 data in the range $5.5 \leq Q^2 \leq 38$ GeV^2. The comparison is done for for four fixed $x = 0.00421, 0.0075, 0.0133$ and 0.0237 respectively.

From the figures we observe that our results of Q^2 and x-evolutions of deuteron

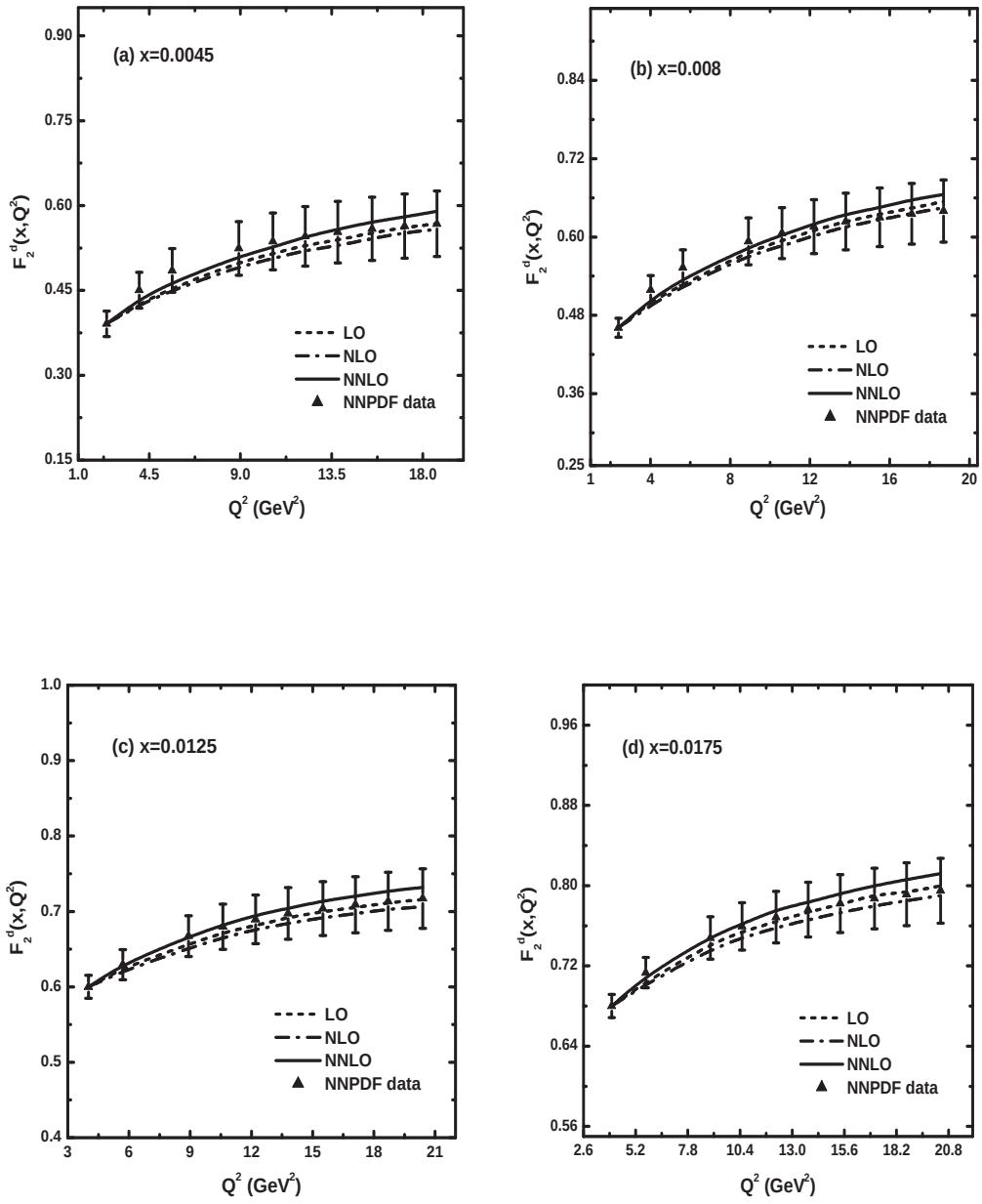

Figure 3.6: Comparison of Q^2 evolution of deuteron structure functions at LO, NLO and NNLO with the NNPDF data for four fixed values x. The dot lines represent the LO results (Eq.3.46), dash-dot lines represent the NLO results (Eq.3.63) and solid lines represent the NNLO results Eq.(3.82).

and proton structure functions are in good consistency with the experimental data and parametrizations. Our predictions at NNLO provide better agreement than LO and NLO results, nevertheless, the difference between the LO, NLO and NNLO results is small. From our analysis in can be anticipated that the region of validity of our method is approximately in the range $10^{-3} \leq x \leq 10^{-1}$ and $0.5 \leq Q^2 \leq 40$

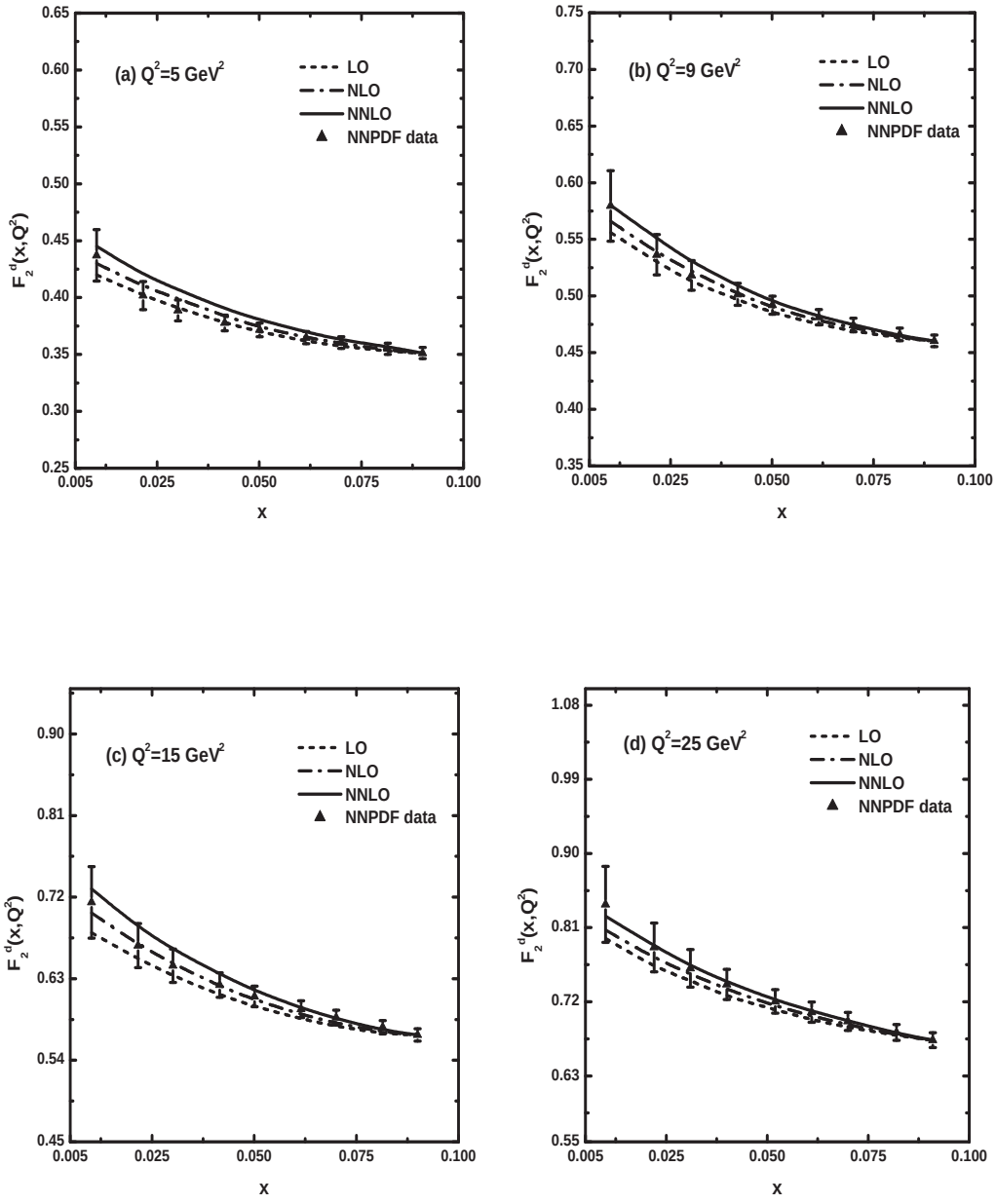

Figure 3.7: Plots showing the comparison of x evolution of deuteron structure function at LO, NLO and NNLO with the NNPDF data for four fixed values of Q^2. The dot lines represent the LO results (Eq.3.47), dash-dot lines represent the NLO results (Eq.3.64) and solid lines represent the NNLO results Eq.(3.83).

GeV^2. But this method may also applicable for other ranges of x and Q^2. Though various methods like Laguerre polynomials [38, 39], Brute-Force method [40], Matrix method [41], Mellin transformation [42, 43] etc. are available in order to obtain a numerical solution of DGLAP evolution equations, our method to solve these equations analytically is also a workable alternative. Here we consider a parameter $K(x)$

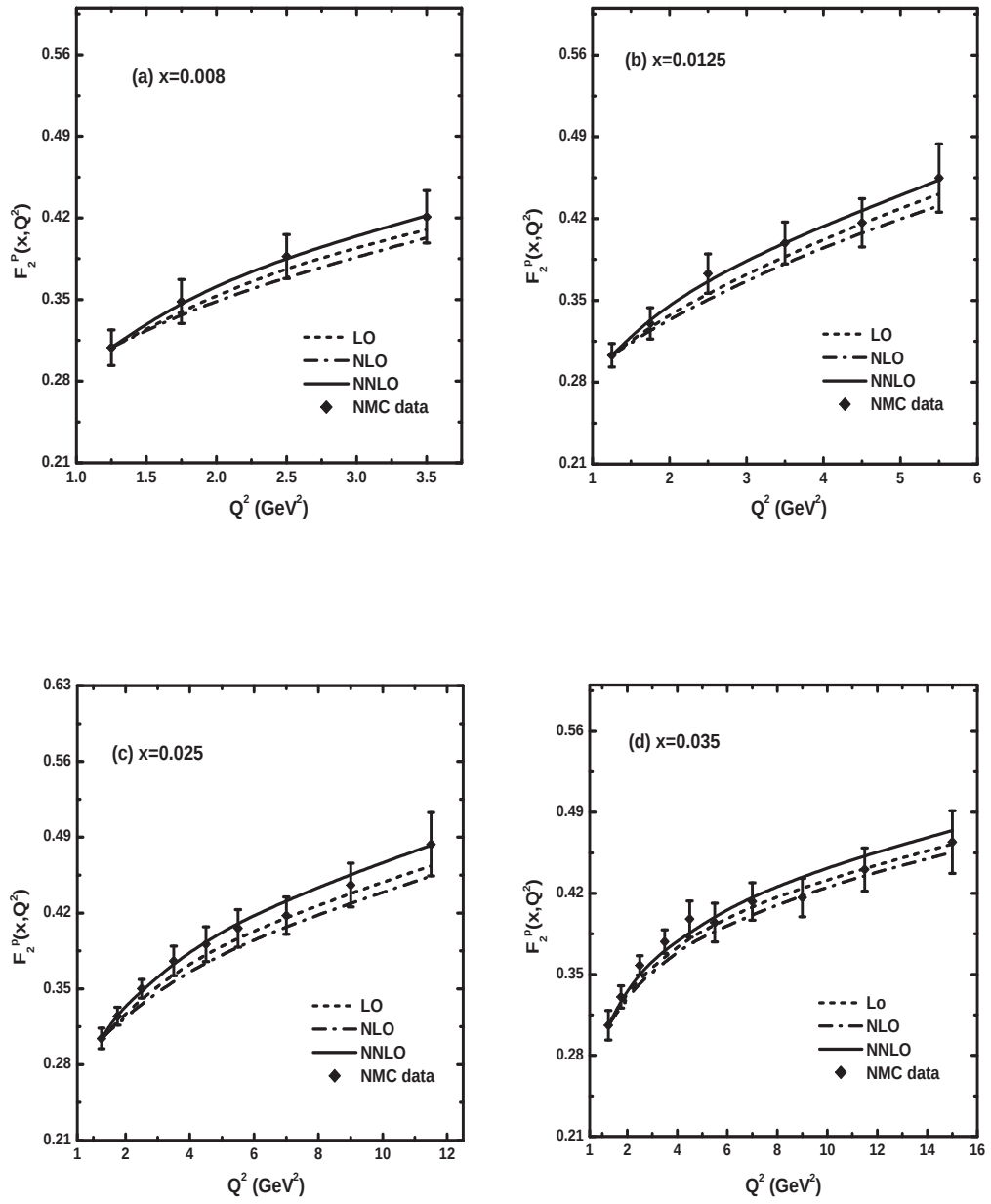

Figure 3.8: Plots of proton structure function at LO, NLO and NNLO vs. Q^2 compared with the NMC data for four particular values of x. The dot lines represent the LO results (Eq.3.48), dash-dot lines represent the NLO results (Eq.3.67) and solid lines represent the NNLO results Eq.(3.88).

in assuming a relation between singlet structure function and gluon parton densities. We have also used two other parameters like T_0 and T_1. However the number of parameters used here are less in comparison to the numerical methods where several parameters have been used mainly in input functions [55, 56]. Moreover, with this method we can calculate the x-evolutions of deuteron structure function in addition

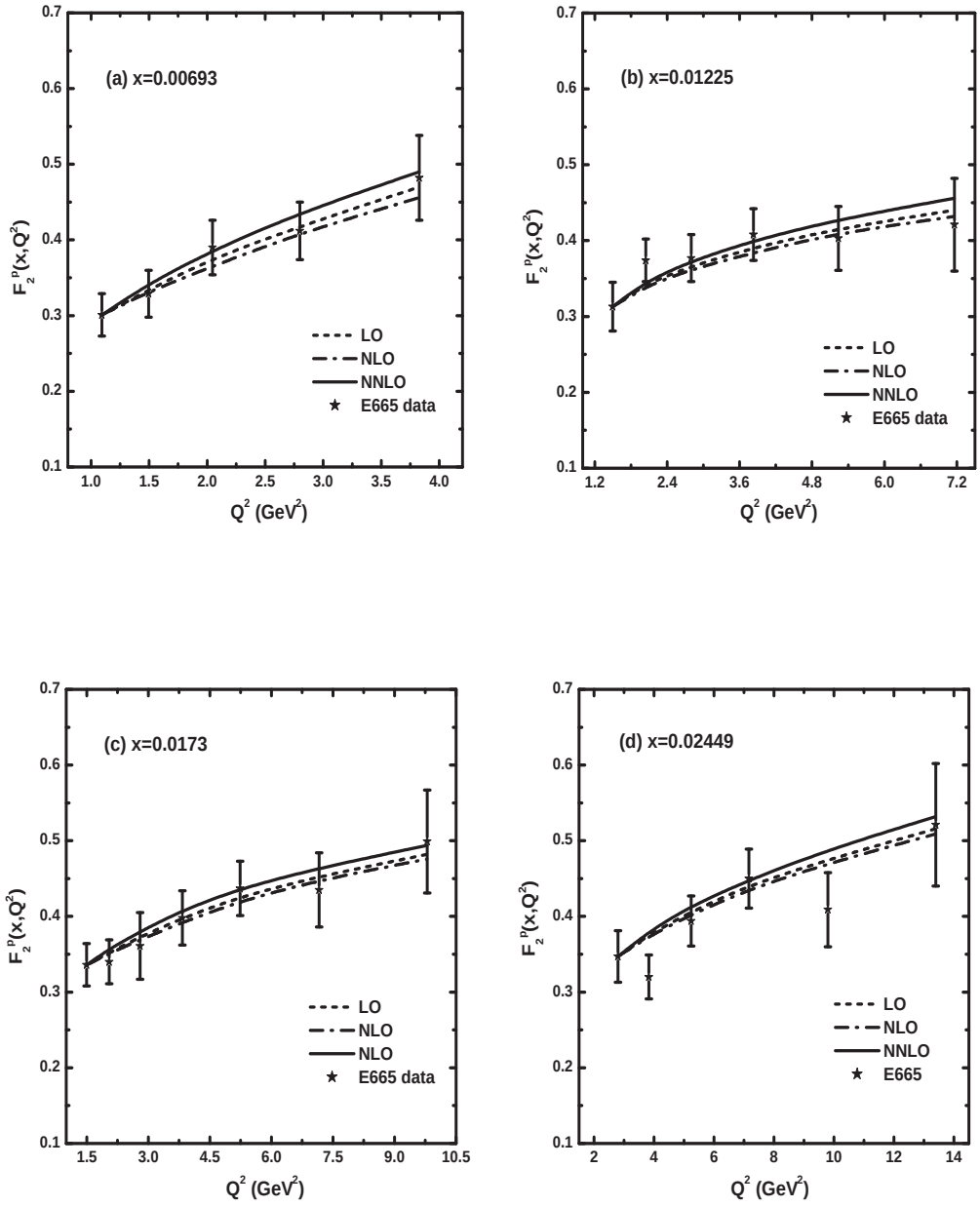

Figure 3.9: Plots showing the comparison of Q^2 evolution of proton structure function at LO, NLO and NNLO with the E665 data for four fixed x. The dot lines represent the LO results (Eq.3.48), dash-dot lines represent the NLO results (Eq.3.67) and solid lines represent the NNLO results Eq.(3.88).

to the t-evolutions.

For a quantitative estimate of the goodness of fit of our results with the experimental data and parametrizations, we perform a χ^2 test. In table 1 we present the χ^2 values for the solutions of deuteron structure function at LO, NLO and NNLO respectively. We observe that our analtical solutions of the deuteron structure function at

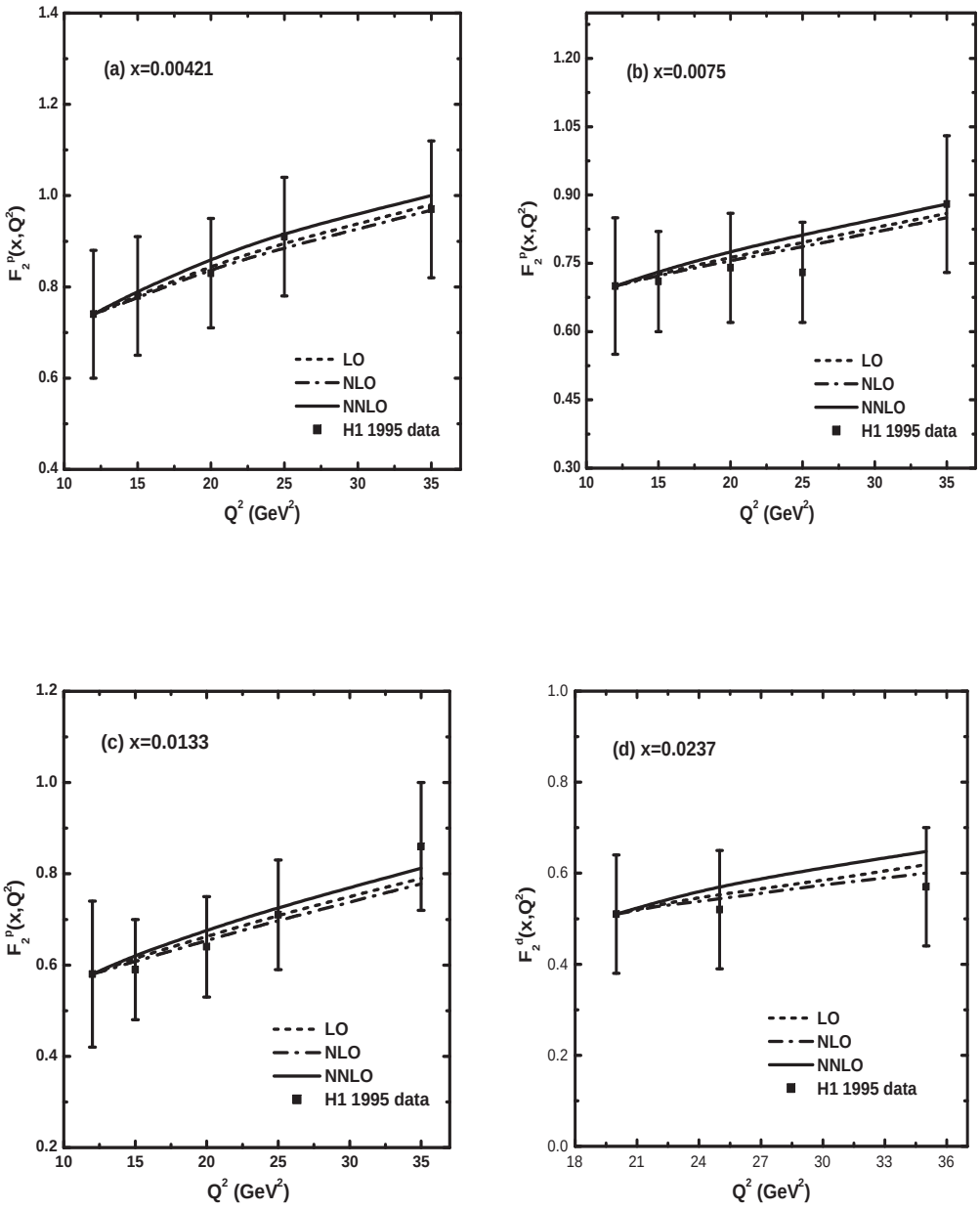

Figure 3.10: Comparison of Q^2 evolution of proton structure function at LO, NLO and NNLO with the H1 1995 data for four fixed x. The dot lines represent the LO results (Eq.3.48), dash-dot lines represent the NLO results (Eq.3.67) and solid lines represent the NNLO results Eq.(3.88).

Table 3.1: χ^2 values for $F_2^d(x, Q^2)$

Order	**NMC**	**E665**	**NNPDF**
LO	3.943	2.215	1.396
NLO	1.733	1.873	0.783
NNLO	1.142	2.07	0.656

LO, NLO and NNLO respectively are in good agreement with the experimental data and parametrizations. However the NNLO results are found to be more compatible.

Table 3.2: χ^2 values for $F_2^p(x, Q^2)$

Order	**NMC**	**E665**	**H1**
LO	2.235	2.477	0.226
NLO	1.097	2.62	0.141
NNLO	0.824	1.92	0.361

Similarly table 2 shows the χ^2 values for the solutions of the proton structure function at LO, NLO and NNLO. Here also we find that our results of proton structure function at LO, NLO and NNLO are almost comparable with the experimental data and parametrizations, nevertheless the NNLO results are more consistent.

3.4 Summary

The Taylor approximated DGLAP equations for the singlet and non-singlet structure functions are solved analytically at LO, NLO and NNLO by the Lagrange's auxilliary method. We also calculate the Q^2 and x-evolutions of deuteron structure function as well as the Q^2-evolution of proton structure function from the solutions of singlet and non-singlet structure functions. The Taylor series expansion changes the integro-differential DGLAP equations into first order partial differential equations which are much easier to solve. This method is comparatively simple and less time consuming for the numerical calculations. We adopt two numerical parameters T_0 and T_1 to evaluate the Q^2 and x-evolutions of singlet and non-singlet structure functions. We also consider the function $K(x) = K$, where K is a constant parameter to relate the singlet and gluon distribution functions and find that K lies in the range $0.45 < K < 1.6$, for our results to be comparable with experimental data and parametrizations. Nevertheless the number of parameters are very few compared to the numerical methods where several parameters are included mainly in the input function. Moreover, with this approch we can calculate the x-evolution of deuteron structure function in addition to the t-evolution. Thus, although various numerical methods are available in order to obtain a numerical solution of DGLAP evolution equations, our approach to solve these equations analytically is also a viable alterna-

tive.

We compare our predictions with the NMC data, E665 data, H1 data as well as with the results of NNPDF parametrization. From our phenomenological analysis we observe that our predicted solutions can explain the general trend of data in a decent manner. Moreover, the inclusion of NNLO contributions provides excellent consistency with the experimental data and parametrizations. Our results show that at fixed x the structure functions increase with increasing Q^2, whereas at fixed Q^2 the structure functions increase with decreasing x which is in agreement with perturbative QCD fits at small-x. By analysing our results we can anticipate that our solutions are valid vis-a-vis the data and parametrizations in the small-x region, roughly in the region $10^{-3} < x < 10^{-1}$. However, our method may loose its validity at very small-x where recombination of gluons have to be taken into account, since these higher order corrections are not included in the derivation of linear DGLAP equations.

Bibliography

[1] Gribov, V. N., Lipatov, L. N. Deep inelastic *ep* scattering in perturbation theory, *Sov. J. Nucl. Phys.* **15**(4), 438−−450, 1972.

[2] Gribov, V. N., Lipatov, L. N. e^+e^- pair annihilation and deep-inelastic *ep* scattering in perturbation theory, *Sov. J. Nucl. Phys.* **15**(4), 675−−684, 1972.

[3] Dokshitzer, Y. L. Calculation of structure functions of deep-inelastic scattering and e^+e^- annihilation by perturbation theory in quantum chromodynamics, *Sov. Phys. JETP* **46**(4), 641−−652, 1977.

[4] Altarelli, G., Parisi, G. Asymptotic freedom in parton language, *Nucl. Phys. B* **126**(2), 298−−318, 1977.

[5] Pascaud, C., Zomer, F. A Fast and precise method to solve the Altarelli-Parisi equations in x space, *arXiv:hep-ph/0104013v1.*

[6] Hirai, M., Kumano, S. and Miyama, M. Numerical solution of Q^2 evolution equations for polarized structure functions, *Comput. Phys. Commun.* **108**(1), 38−−55, 1998.

[7] Coriano, C., Savkli, C. QCD evolution equations: Numerical algorithms from the Laguerre expansion, *Comput. Phys. Commun.* **118**,(2-3), 236−−258, 1999.

[8] Botje, M. A QCD analysis of HERA and fixed target structure function data, *Eur. Phys. J. C* **14**(2), 285−−297, 2000.

[9] Ratcliffe, P. G. Matrix Approach to a numerical solution of the Dokshitzer-Gribov-Lipatov-Altarelli-Parisi evolution equations, *Phys.Rev. D* **63**(11), 116004, 2001.

[10] Cafarella, A., Coriano, C. and Guzzi, M. NNLO logarithmic expansions and exact solutions of the DGLAP equations from x-space: New algorithms for precision studies at the LHC, *Nucl. Phys. B* **748**(1-2), 253−−308, 2006.

[11] Abbott, L. F., Atwood, W. B. and Barnett, R. M. Quantum-chromodynamic analysis of eN deep-inelastic scattering data, *Phys. Rev. D* **22**(3), 582−−593, 1980.

[12] Furmanski, W., Petronzio, R. Lepton-hadron processes beyond leading order in quantum chromodynamics, *Z. Phys. C* **11**(4), 293−−314, 1982.

[13] Ball, R. D., Forte, S. A direct test of perturbative QCD at small x, *Phys. Lett., B* **336**(1), 77−−79, 1994.

[14] Kotikov, A. V., Parente, G. Small x behavior of parton distributions with soft initial conditions, *Nucl. Phys. B* **549**(1-2), 242−−262, 1999.

[15] Sarma, J. K., Choudhury, D. K. and Medhi, G. K. x-distribution of deuteron structure function at low-x, *Phys.Lett. B* **403**(1-2), 139−−144, 1997.

[16] Sarma,J. K., Das, B. t evolutions of structure functions at low-x, *Phys. Lett. B* **304**(3-4), 323−−328, 1993

[17] Choudhury, D. K., Deka, Ranjita and Saikia, A. Gluon distribution and $\frac{dF_2}{d\ln Q^2}$ at small x in the next-to-leading order, *Eur. Phys. J. C* **2**(2), 301−−305, 1998.

[18] Choudhury, D. K., Sahariah, P. K. A solution of the DGLAP equation for gluon at low x, *Pramana J. Phys.* **58**(4), 599−−610, 2002.

[19] Baishya, R., Sarma, J. K. Method of characteristics and solution of DGLAP evolution equation in leading and next to leading order at small x, *Phys. Rev. D* **74**(10), 107702, 2006.

[20] Baishya, R., Sarma, J. K. Semi numerical solution of non-singlet Dokshitzer-Gribov-Lipatov-Altarelli-Parisi evolution equation up to next-to-next-to-leading order at small x, *Eur. Phys. J. C* **60**(4), 585−−591, 2009.

[21] Baishya, R., Jamil, U. and Sarma, J. K. Evolution of spin-dependent structure functions from DGLAP equations in leading order and next to leading order, *Phys. Rev. D* **79**, 034030, 2009.

[22] Choudhury, D. K., Islam, S. An analysis of non-singlet structure function in next-to-next-to-leading order at small-x, *Indian J. Phys.* **85**(2), 319−−328, 2011.

[23] Arneodo, M. et al., Measurement of the proton and deuteron structure functions, F_2^p and F_2^d, and of the ratio σ_L/σ_T, *Nucl. Phys. B* **483**,(1-2), 3−−43, 1997.

[24] Adams, M. R. et al., Proton and deuteron structure functions in muon scattering at 470 GeV, *Phys. Rev. D* **54**(5), 3006−3056, 1996.

[25] Ahmed, T. et al., A measurement of the proton structure function $F_2(x,Q^2)$, *Nucl. Phys. B* **439**(3), 471−−502, 1995.

[26] Forte, S. et al., Neural network parametrization of deep inelastic structure functions, *JHEP* **2002**(JHEP05), 062, 2002.

[27] Halzen, F., Martin, A. D. *Quarks and Leptons: An Introductory Course in Modern Particle Physics*, John Wiley and Sons, Canada, 1984.

[28] Van Neerven, W. L., Vogt, A. NNLO evolution of deep-inelastic structure functions: the singlet case, *Nucl. Phys. B* **588**(1-2), 345−−373, 2000.

[29] Van Neerven, W. L., Vogt, A. NNLO evolution of deep-inelastic structure functions: the non-singlet case, *Nucl. Phys. B* **568**(1-2), 263−−286, 2000.

[30] Moch, S., Vermaseren, J. A. M. and Vogt, A. The three-loop splitting functions in QCD: the non-singlet case, *Nucl. Phys. B* **688**(1-2), 101−−134, 2004.

[31] Vogt, A., Moch, S. and Vermaseren, J. A. M. The three-loop splitting functions in QCD: the singlet case, *Nucl. Phys. B* **691**(1-2), 129−−181, 2004.

[32] Shaikhatdenov, B. G. et al., QCD coupling constant at next-to-next-to-leading order from DIS data, *Phys. Rev. D* **81**(3), 034008, 2010.

[33] Martin, A. D. et al., Parton distributions for the LHC, *Eur. Phys. J. C* **63**(2), 189−−285, 2009.

[34] Furmanski, W., Petronzio, R. Singlet parton densities beyond leading order, *Phys. Lett. B* **97**(3-4), 437−−442, 1980.

[35] Curci, G., Furmanski, W. and Petronzio, R. Evolution of parton densities beyond leading order: The non-singlet case, *Nucl. Phys. B* **175**(1), 27−−92, 1981.

[36] Benvenuti, A. C. et al., A high statistics measurement of the deuteron structure functions $F_2(x, Q^2)$ and R from deep inelastic muon scattering at high Q^2, *Phys. Lett. B* **237**(3-4), 592−−598, 1990.

[37] Adloff, C. et al., Measurement and QCD analysis of neutral and charged current cross sections at HERA, *Eur. Phys. J. C* **30**(1), 1−−32, 2003.

[38] Coriano, C., Savkli, C. QCD evolution equations: Numerical algorithms from the Laguerre expansion, *Comput. Phys. Commun.* **118**(2-3), 236−−258, 1999.

[39] Schoeffel, L. An elegant and fast method to solve QCD evolution equations. Application to the determination of the gluon content of the Pomeron, *Nucl. Instrum. Methods A* **423**(2-3), 439−−445, 1999.

[40] Hirai, M., Kumano, S. and Miyama, M. Numerical solution of Q^2 evolution equations for polarized structure functions, *Comput. Phys. Commun.* **108**(1), 38−−55, 1998.

[41] Ratcliffe, P. G., A matrix approach to numerical solution of the DGLAP evolution equations, *Phys. Rev. D*,**63**(11), 116004, 2001.

[42] Kosower, D. A., Evolution of parton distributions, *Nucl. Phys. B* **506**(1-2), 439−−467, 1997.

[43] Weinzierl, S., Fast evolution of parton distributions, *Comput. Phys. Commun.* **148**(3), 314−−326, 2002.